ORIGINAL PAPER

Gas–Liquid Chemical Reactions with Nanosecond Pulses: Role of Frequency and Pulse Delivery Modes

Radha Krishna Murthy Bulusu[1] · Nina Mihajlov[1] · Christopher W. Patterson[1] · Robert J. Wandell[1] · Bruce R. Locke[1]

Abstract

The effects of changes in the mode of delivery of nanosecond pulses in a gas–liquid plasma reactor on the formation of hydrogen peroxide, H_2O_2, and, as an indicator for ·OH radicals, the decoloration of methylene blue, MB, were determined for pulse delivery by (a) increasing frequency with uniform pulses (5–50 kHz), (b) variation of the time between bursts of pulses (burst period), (c) changing the inner burst frequency (1 over the time between the pulses in the burst), and (d) variation of number of pulses in a burst (N-cycles). H_2O_2 peroxide formation was not affected by the method of pulse delivery in the range of parameters studied here and all data followed an approximately linear increase in H_2O_2 production rate with discharge power. In contrast, the MB decoloration rate was affected by the burst modes. In terms of discharge power, the MB decoloration rate was highest for the uniform pulse mode; however, the linear trend in increase of MB decoloration with power when the burst period was varied, suggest that at higher power the burst mode may be more effective than the uniform pulsing. Consideration of the per pulse decoloration with energy per pulse and with number of pulses suggest that the burst mode can affect reactions differently from applying a uniform pulse.

Keywords Gas-liquid plasma reactors · Nanosecond pulsed discharges · Pulse burst mode · Hydrogen peroxide · Methylene blue

Introduction

Electrical discharge plasma formed in contact with liquid water is of interest for applications in chemical, biomedical, agricultural, electrical, and materials engineering [1–3]. A wide range of different types of gas–liquid nonthermal plasma reactors that use various power supplies such as DC, AC, microwave, radiofrequency, and pulsed have been developed and tested. Of significant current interest is the utilization of nano-second pulsed discharges to synthesize chemical products such as hydrogen peroxide (H_2O_2) from water [4] and nitrate and nitrite using water with air as a carrier gas [5]. While research on the effects

---

✉ Bruce R. Locke
  locke@eng.famu.fsu.edu; blocke@fsu.edu

1   Department of Chemical and Biomedical Engineering, FAMU-FSU College of Engineering, Florida State University, Tallahassee, FL 32310, USA

of variation of the pulse properties to control plasma chemistry in general has been conducted, limited work has been reported to modify the waveforms and pulse delivery modes in gas–liquid plasma chemical reactors. Examples in gas-phase plasma chemistry include pulse discharge control for ozone generation [6], waveform tailoring in plasma etching [7], waveform tailoring in gas phase spark channels for oxygen atom formation [8], pulse shape effects on hydroxyl radical, ·OH, production [9], and pulse shape effects on methane reforming in micro-dielectric barrier discharges [10]. The effects of frequency on plasma properties have been considered [11], and the role of burst mode operation in plasma jets for bacteria inactivation in wounds have been studied [12]. The effects of residual electrons and plasma conductivity on sequential pulses in a helium plasma jet with nanosecond bursts [13] and the enhancement of atomic hydrogen radical, ·H, by bursts of nanosecond pulses in such plasma jets [14] have been reported. In one of the few reported studies on the effects of the pulse delivery mode in gas–liquid plasma chemistry, Gromov et al. demonstrated ·OH enhancement in nitrogen fixation in a burst of three pulses generated over a water surface [15].

In order to focus on an element of a filamentary plasma channel propagating along a gas–liquid water interface, we developed a small, tubular reactor [16, 17] that allows for control of the gas and liquid flows, measurement of the interfacial area and gas and liquid volumes, and determination of transport and plasma properties. The chemical reactions analyzed in this reactor (all for cases of uniform pulse delivery) include H_2O_2 formation [18, 19], hydrocarbon [20] and organic dyes [21] oxidation, degradation of organic contaminants combined with bioreactors [22], nitrogen oxides (NO, NO_2, NO_3^-, NO_2^-) formation [23, 24], hydroxyl radical (·OH) generation [25], degradation of fluorinated compounds [26, 27], formation of molecular hydrogen (H_2) [28], and formation of aqueous electrons (e^-_{aq}) [29]. Time averaged optical emission spectroscopy (OES) provided average electron density and plasma gas temperature [6, 7]. Time resolved electron density during a single pulse by OES demonstrated the roles of pulse frequency and pulse width on the plasma electrons, which were correlated to the formation of H_2O_2 and the peak electron density correlated to the degradation of fluorinated surfactants (perfluorooctanoic acid—PFOA) [27].

In this previous work we have shown that the properties of the single pulse (e.g., risetime, pulse width, input voltage) with uniformly varied frequency can influence the energy yield/efficiency of various chemical reactions occurring in the reactor by changing the plasma properties (plasma gas temperature, electron density, electron energy) [16, 17, 20, 24, 28]. However, optimization of a chemical reactive system with these parameters alone is limited due to the significantly different time scales of the plasma interactions as compared to the time scales of the reactive chemistry and mass transfer between the gas and liquid phase. Therefore, present study seeks to determine how the delivery of nanosecond pulses in bursts affects the H_2O_2 production and, as a measure of ·OH formation, methylene blue dye decoloration, as commonly used in plasma gas–liquid reactors [21, 30].

Methods

Experimental Set-up

The experimental set-up used in this study is shown in Fig. 1 and is the same as used in previous work [17, 27]. In all experiments the carrier gas was argon (60 psi). Deionized water with an initial pH of 6.04 and a conductivity of 14.1 μ S/cm were utilized for the H_2O_2 production experiments. For the methylene blue (MB) decoloration experiments,

0.5 mM aqueous MB solutions were prepared from deionized water with a resulting pH of 6.2 and conductivity of 112 μ S/cm. The liquid feed streams were supplied to the reactor using a high-pressure reciprocating pump (Optos Series, Eldex Laboratories, Napa, CA) and the flowrates used were 2 mL/min for all H_2O_2 experiments and 5–15 mL/min for the MB decoloration experiments. Before entering the reactor, the gas and the liquid streams enter a mixing zone and are then fed through a stainless-steel inlet capillary (0.25 mm ID) to the cylindrical reaction zone (4 mm height, 3 mm diameter). The reaction zone is located inside a quartz block of 2.5 cm×2.5 cm×1.3 cm as shown in Fig. 1. The liquid flows along the internal reactor walls and the gas flows through the central core while the plasma channel propagates along the gas–liquid interface as depicted in the picture in the bottom right of Fig. 1 and in our previous work [17]. The gas–liquid mixture exits the reactor through a stainless-steel outlet capillary (1 mm ID). The inlet and outlet stainless steel capillary tubes act as electrodes through connections to the pulse forming network [17].

Pulse Forming Network

The nanosecond pulser of the pulse forming network was custom-made by Airity Technologies, LLC (Palo Alto, California) and was the same as used in previous work [27, 28]. The pulser was connected to a function generator (Rigol 1022Z, Portland, OR) which acted as the trigger signal and a variable DC power supply (Sorensen XHR 600–1.7, British Columbia, Canada) for the high voltage input. The Airity power supply has an internal voltage transformation and a pulse stage that provides voltage gains of 100–130 times depending on the load. The pulse rise time of the Airity pulser is 220 ns to peak voltage. The single pulse/uniform pulse operation with this power supply network was discussed in previous work [27].

In this work, burst mode of the function generator was utilized to trigger the Airity pulser to send a train of high frequency bursts of pulses. The time between the bursts
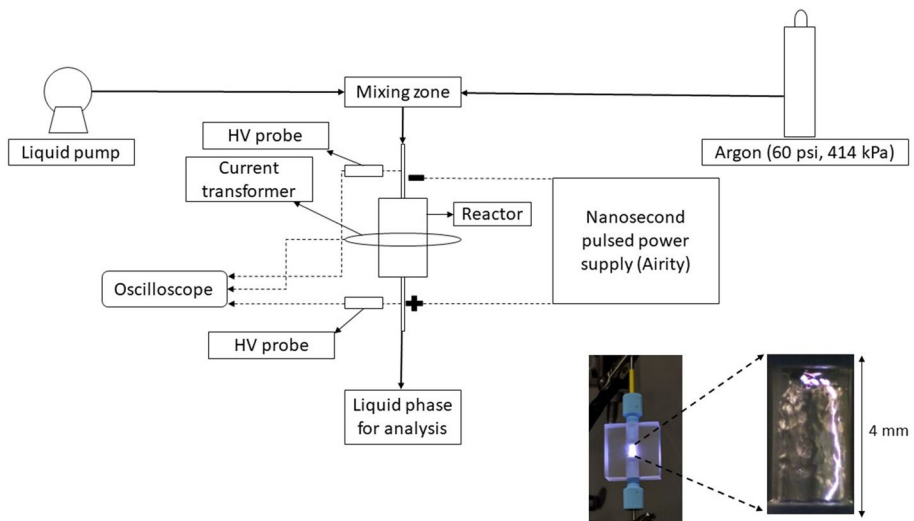

Fig. 1 Experimental set-up showing gas and liquid feed streams into the quartz cell reactor connected to the nanosecond pulsed power supply. Insert shows the reactor cell and a close up of the plasma discharge with a short exposure time photograph

(burst period), the time between the pulses in the burst (internal frequency), and the number of pulses in a burst (N-cycles) were varied using the function generator. Inner burst relaxation time and outer burst relaxation time were varied by changing the internal frequency and burst period, respectively. An Illustration of burst mode voltage/current/power is shown in Fig. 2.

The terminology used in this work shown in Fig. 2 is given by:

- Burst mode—The setting on the function generator that allows a "burst" of high frequency pulses.
- Inner burst frequency/Internal frequency (Inner burst relaxation time) – frequency of the pulses in the burst (for example: at 100 kHz internal frequency, the time (inner burst relaxation time) between the pulses in the burst is 10 μ s).
- Burst period—time between initial strikes of two consecutive bursts.
- N-cycles—number of pulses in a burst.
- Outer burst frequency–frequency of the bursts as a whole.

Electrical Diagnostics

The electrical diagnostic method utilized here is similar to the one used in our previous work [18, 19] with slight modifications to accommodate the burst mode operation. Two high voltage (HV) probes (TektronixP6015A, 1/1000; Beaverton, OR) were connected to the electrodes to measure the voltage difference between the electrodes (reactor inlet and outlet). A current monitor (Pearson Electronics, model 6585; Palo Alto, CA) was positioned around the body of the reactor to measure the current of the formed plasma channels. The voltage and the current probes were connected to an oscilloscope (Tekronix MCO 3014, Beaverton, OR) to determine the energy per burst via the following equation:
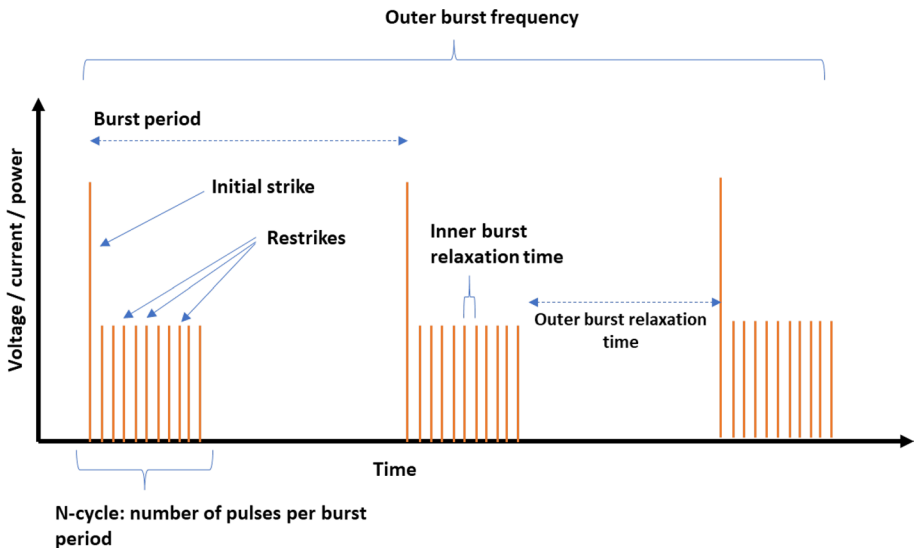

Fig. 2 Illustration of burst mode voltage/current/power waveforms

$$Energy per burst = \int (V \times I) dt \tag{1}$$

where V is the instantaneous voltage, I is the instantaneous current, and t is the time period of the burst. Figure 3 shows the V-I example waveform of one burst with a 100 kHz internal frequency, 1 ms burst period and 10 N-cycles. For each experimental condition, three high resolution measurements of one burst were obtained to calculate an average burst energy and associated error. Total power was then calculated by multiplying the average burst energy with the outer burst frequency.

Chemical Analysis

The liquid effluent exiting the reactor was collected and analyzed to determine H_2O_2 concentration and MB decoloration for the various experiments conducted. A colorimetric test using titanium oxysulfate sulfuric acid complex and UV–Vis spectroscopy (Lambda 35, PerkinElmer, Waltham, MA) was used to determine H_2O_2 concentration [31]. The MB concentration was also determined using UV–Vis spectroscopy from the absorbance band of the molecule at 664 nm. A calibration curve (see supplementary data) was prepared with serial dilution of a stock solution of 0.5 mM MB. Conductivity and pH were determined for all solutions using a conductivity probe (Cond 6+, Oakton Instruments, Vernon Hills, IL) and a pH probe (HACH, Loveland, Colorado); values for these measures data can be found in the supplementary data.
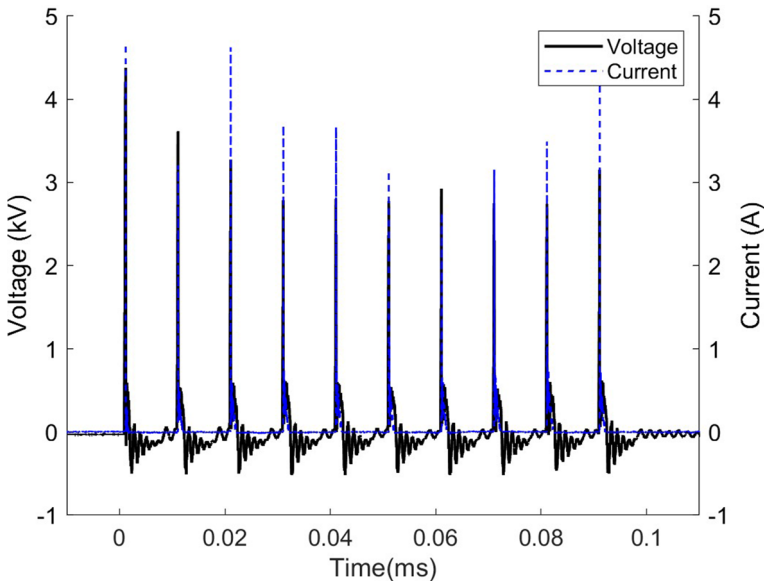

Fig. 3 Voltage and current waveform example for 100 kHz internal frequency (10 μ s between pulses in the burst), 1 ms burst period and 10 N-cycles

Table 1 Burst mode parameters used for H_2O_2 experiments

Case #	Internal frequency (kHz)	Burst period (ms)	N-cycles
Burst mode, Case I	100–400	1	5
Burst mode, Case II	100	0.1–1	5
Burst mode, Case III	100	1	1–40

Table 2 Burst mode parameters used for MB decoloration experiments

Case #	Internal frequency (kHz)	Burst period (ms)	N-cycles
Uniform pulse	5–50	NA	NA
Burst mode, Case I	50–300	0.5	10
Burst mode, Case II	100	0.25–1	10
Burst mode, Case III	100	1	1–30

Experimental Conditions

Three sets of experiments were conducted to determine the effect of burst mode on H_2O_2 formation as shown in Table 1. The first burst mode, Case I, involves variation of the internal frequency between the individual pulse strikes from 100 to 400 kHz. The second burst mode, Case II, varies the burst period, i.e., the time between each burst from 0.1 to 1 ms. Case III varies the N-cycles, or the number of pulses in a burst from 1 to 40. Each set of experiments was conducted with a 2 mL/min DI water flowrate and a 45 V DC input voltage to the pulser, i.e., 5.1 kV of input voltage.

Four sets of experiments were conducted to determine the effects of burst mode on MB decoloration as shown in Table 2. The first is the uniform pulse case where the overall pulse frequency was varied from 5 to 50 kHz. The first burst mode, Case I, involves variation of the internal frequency between individual pulse strikes from 50 to 300 kHz. The second burst mode, Case II, varies the burst period, i.e., the time between each burst from 0.25 to 1 ms. Case III varies the N-cycles, or the number of pulses in a burst from 1 to 30. Each set of experiments was conducted for three different flowrates; 5, 10, and 15 mL/min. For all MB experiments a 50 V DC input voltage to the pulser was utilized i.e., 5.6 kV of input voltage.

Results and Discussion

Discharge Power

A.   Methylene Blue (MB)

 Figure 4 shows the total discharge power for the different conditions for all cases. For the uniform pulsing the total discharge power increased linearly with an increase in frequency from 5 to 50 kHz which follows similar trends in previous work [28]. In contrast, the power

values decreased with an increase in the internal frequency for the Burst mode Case I, due to the "memory effect" [32], where there are charged particles (such as free electrons, positive ions, metastable species, etc.) remaining from the initial plasma strike which reduces the breakdown voltage required to initiate formation the next plasma channel (restrike). It should also be noted that the "restrikes" occur in the same spatial location in the reactor as the "initial strike". The most energy is needed for the "initial strike" breakdown voltage to happen, after which, for successive restrikes, less total energy is needed as indicated by the reduced breakdown voltage and the current dissipated of each following restrikes. Therefore, the energy in each "restrike" is over an order of magnitude smaller than that of the "initial strike", this results in lower power values as the internal frequency increases and this phenomenon is exacerbated. As the burst period increases, Case II, the overall burst frequency decreases. The total discharge power increased with an increase in the N-cycles, Case III, due to the increase in number of pulses in a burst. For all cases, it can be observed that the liquid flowrate does not have a significant effect on power. As shown in the supplementary data, there was no significant difference in total discharge power between 0.5 mM MB solution and DI water. This is consistent with our previous work [19] because the increase in conductivity was minimal. i.e., 14.1–112 μ S/cm.

b. Hydrogen peroxide

Figure 5 shows the total discharge power as functions of the different burst mode variables for all burst mode cases for production of H_2O_2. As shown in Fig. 5a, the total discharge power decreases from 0.61 to 0.37 W when the internal frequency was varied between 100 and 400 kHz at constant 1 ms burst period and 5 N-cycles. The reason for this decrease is explained by the memory effect described in the previous Sect. 3.1.a. As the burst period increases, Case II, the overall burst frequency decreases. The total discharge power increased with an increase in the N-cycles, Case III, due to the increase in number of pulses in a burst. Power measurements for the H_2O_2 production experiments are shown in Fig. 5. The DC input voltage used for the H_2O_2 study was 45 V i.e., 5.1 kV. This resulted
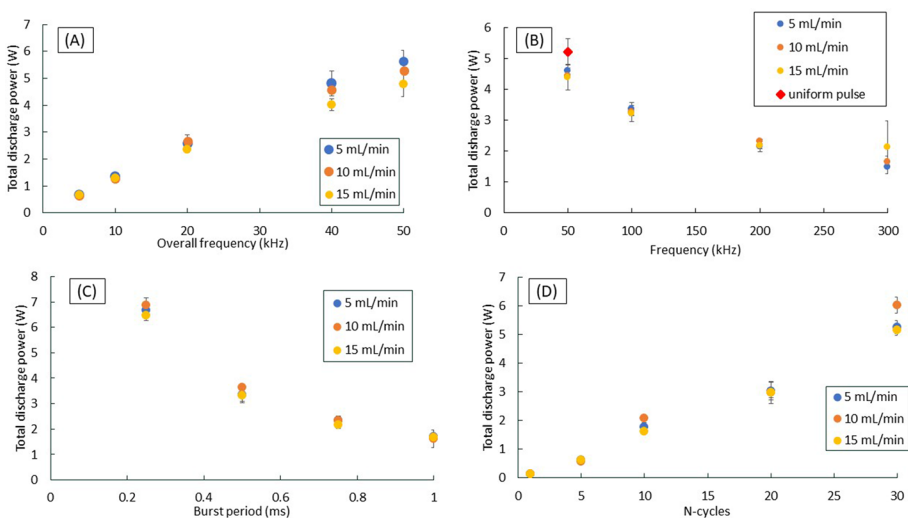

Fig. 4 Discharge power for the different cases of MB a uniform frequency, b Case I, c Case II, d Case III

in less total discharge power when compared with 50 V, i.e., 5.6 kV used for the MB study but overall similar trends with variation of burst variables.

Hydrogen Peroxide Formation

H_2O_2 formation in the uniform pulse case has been previously reported [18, 27, 28] where there is a linear increase with frequency up to a specific value (approximately 10 kHz) and thereafter a leveling off of the production at higher frequency. The leveling off of production at higher frequency has been attributed to back reactions that lead to the degradation of H_2O_2 by radical reactions [28].

Figure 6 shows the H_2O_2 production rates and energy yields for the three burst mode cases. In Case I, the production rate and energy yield are not strong functions of the internal frequency although a maximum in energy yield is found at about 300 kHz. For Case II, the production rate decreases with burst period, which is consistent with the lower power, but the energy yield also drops. In Case III, the production rate increases linearly with the N-cycles. Due to a similar trend of power linearly increasing with N-cycles, the energy yield is approximately constant.

Figure 7 shows the data for all cases in terms of the H_2O_2 production rate with total power. The uniform pulse data shown here is from our previous study [27]. The burst mode results follow the same trend as the uniform pulse demonstrating that the implementation of the various types of bursts does not have a significant effect on the H_2O_2 production rate. Plotting the data on a per pulse basis against the energy per pulse as in Fig. 8 also demonstrates that H_2O_2 production in each pulse is correlated with the input energy in each pulse and not the means of how the pulse is delivered.
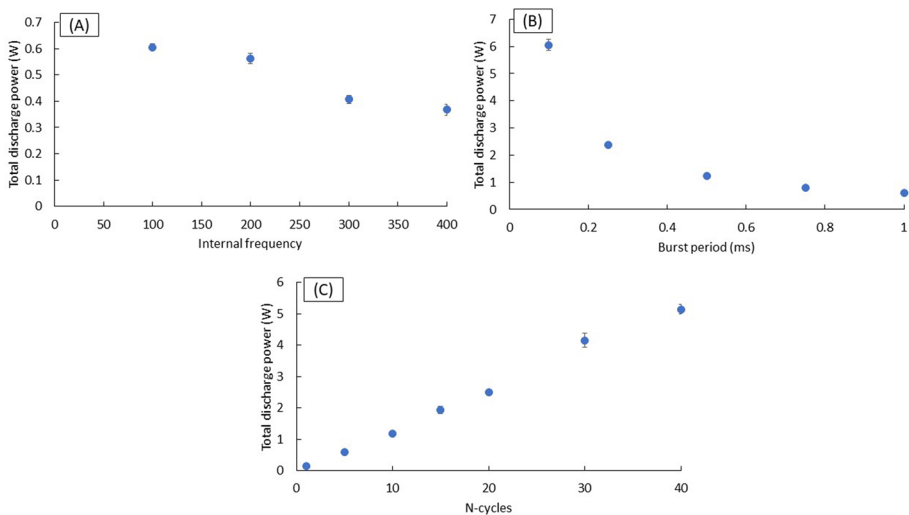

Fig. 5 Discharge power for all cases for H_2O_2 measurements. **a** Case I, **b** Case II, and **c** Case III
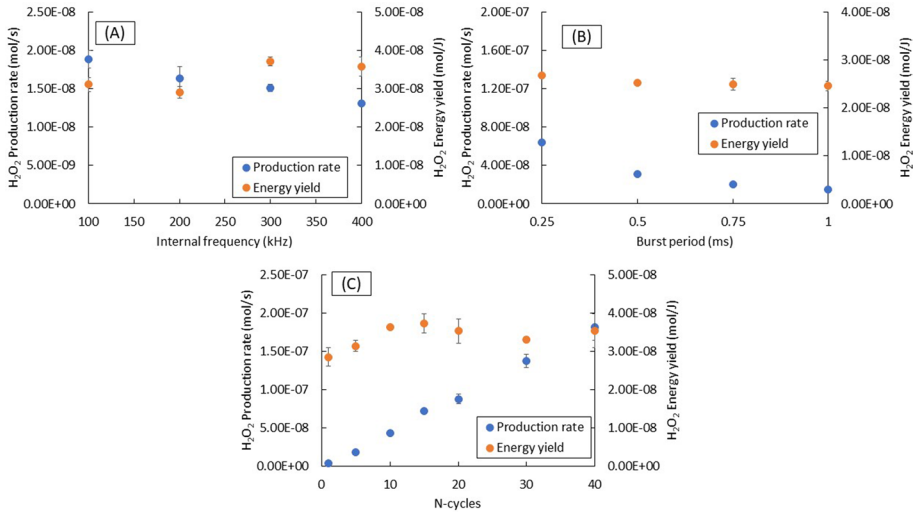
Fig. 6 H_2O_2 production rates and energy yields with **a** Case I—variation of inner frequency with constant 1 ms burst period and 5 N-cycles (pulses in a burst), **b** Case II—burst period at fixed 5 N-cycles (pulses in a burst) and 100 kHz internal frequency and **c** Case III—the number of N-cycles (pulses in a burst) at fixed 1 ms burst period and 100 kHz inner burst frequency
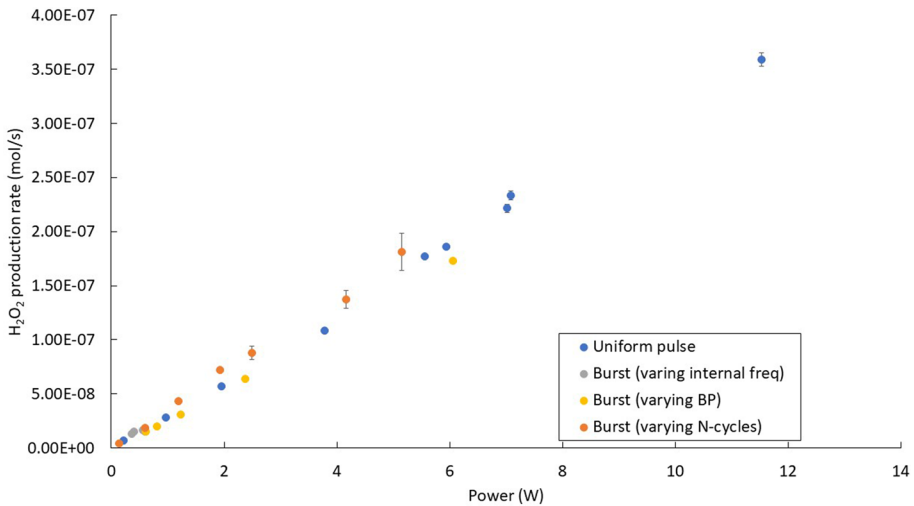

Fig. 7 H_2O_2 production rate of all results with respect discharge power

Methylene Blue (MB)

Figure 9 shows the MB decoloration rates for all cases. The decoloration rate increases approximately linearly with frequency up to 10 kHz for 5 mL/min and 20 kHz for 10 and
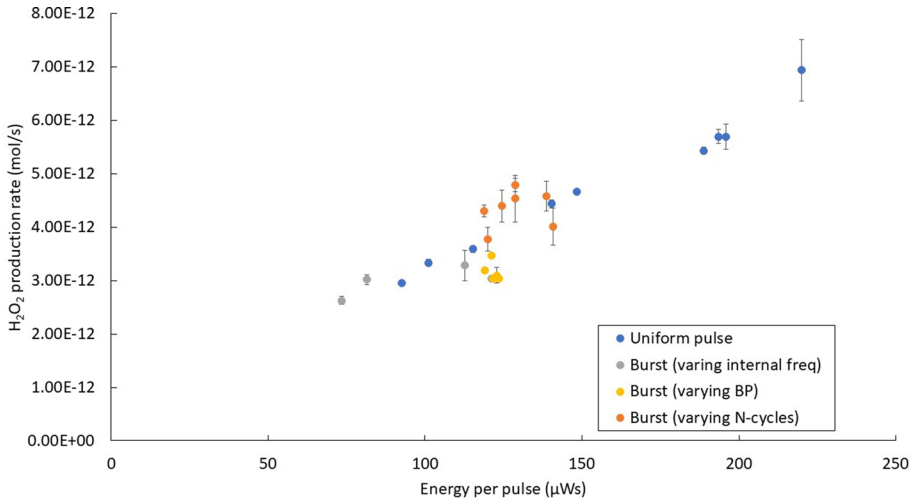
Fig. 8 H_2O_2 production per pulse vs energy per pulse for all the cases suggesting that in the cases where the gas residence time is of similar magnitude to the interpulse period the production rate is approximately constant for the range of energy per pulse

15 mL/min. Thereafter it levels off to constant values at the frequencies above 40 kHz for the uniform pulsing case. The shifting of the frequency from the linear behavior to the saturation behavior at the higher liquid flow rates is consistent with the shorter liquid (and gas) residence times at higher flow rates and shorter inter-pulse periods at higher frequency [17]. The smaller liquid residence time allows for higher production rate at higher frequencies minimizing back reactions that might reduce high reactive species.
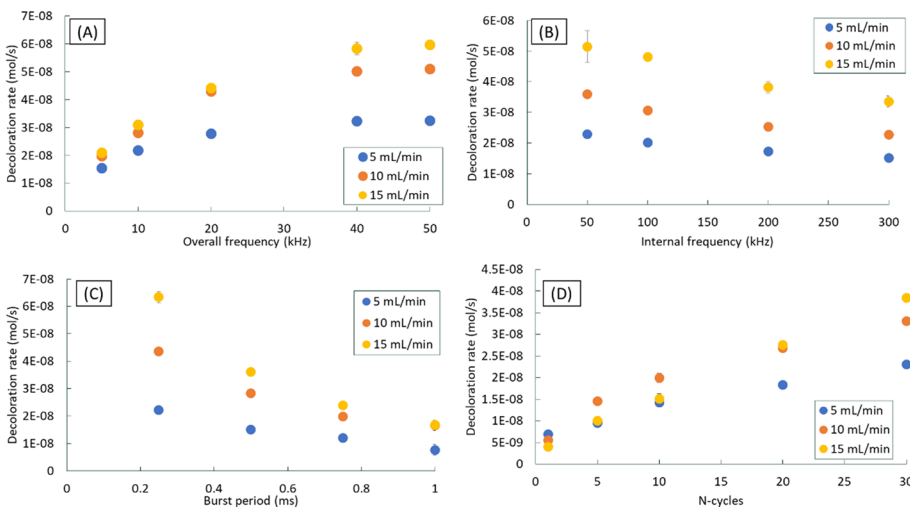
Fig. 9 MB decoloration rates for **a** uniform pulsing, **b** Case I—variation of internal frequency, **c** Case II—variation of burst period, and **d** Case III—Variation of N-cycles

In the burst mode cases, the decoloration rate decreased with an increase in the internal burst frequency, Case I Fig. 8b, because the total discharge power decreased. Similarly, as for the uniform pulse case, when the solution flowrate was increased, the decoloration rate increased as well, since they are directly related. For Case II, the decoloration rate decreased with an increase in the burst period because the total discharge power and the overall frequency decreased with increasing burst periods. For Case III the decoloration rate increased with an increase in N-cycles, as the number of pulses interacting with gas–liquid interface increased.

Figure 10 shows the decoloration rate vs. power data for all the trials at the three flowrates. In contrast to the H_2O_2 results, the implementation of the burst mode affects the decoloration rate of MB. All cases showed an increase in the decoloration rate with an increase in the power, but the burst mode Case II and Case III have linear increases with power and the Case I and uniform pulsing show saturation type behavior at the higher power levels. The overall increase in decoloration with power is consistent with other plasma reactors where more power leads to higher decoloration or degradation. The linear increase in decoloration rate for the Case II and Case III suggests that when the gas residence time is of the same order of magnitude as the burst period, the linear increase with increasing power can be sustained, while in the uniform pulsing case where the gas residence time becomes much larger than the inter-pulse period, there is a saturation behavior. Future work is necessary to explore wider ranges of pulse conditions to determine if the linear trend in Case II can be sustained at higher power and give rise to higher degradation rates than the uniform pulsing. It was not possible to operate the current power network in the burst mode at power levels higher than shown here.

Figure 11 shows the energy yield (EY) vs. power data for all the trials with the three flowrates. All trials showed an approximately exponentially decreasing trend in the energy yield values with an increase in the total discharge power. Generally, the highest EY values were achieved with the uniform pulse case. However, the burst mode, Case III, at low power with an N-cycle of 1, gave the highest overall energy yield but it should be noted that this case is equivalent to using a uniform pulse.
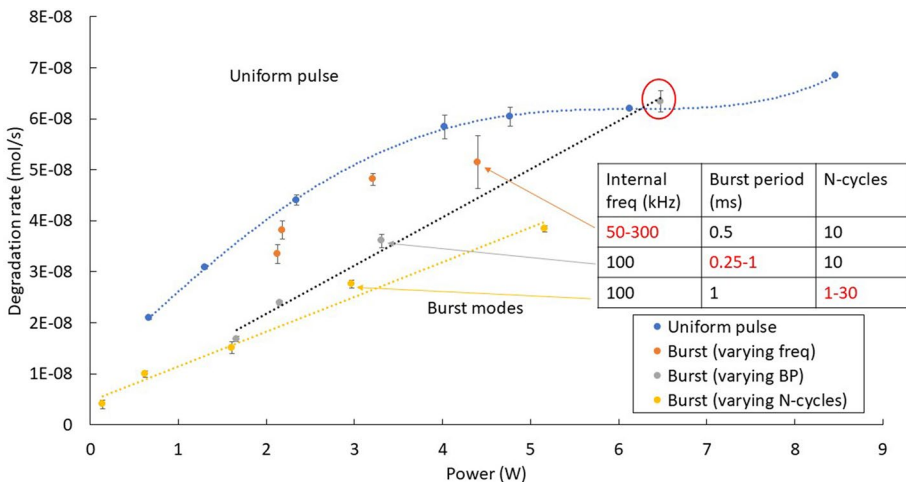

Fig. 10 MB degradation rate with power for uniform pulsing and burst modes
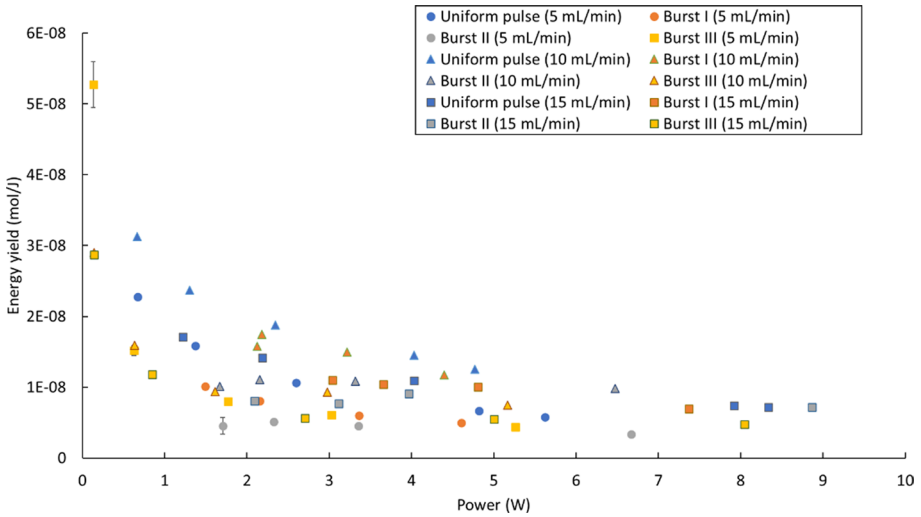
Fig. 11 Energy yield vs. power: combined data of all trials for the three flowrates

Figure 12 shows the decoloration per pulse varying with energy per pulse at a 15 mL/min flowrate. The decoloration per pulse increases with energy per pulse for both uniform pulsing and Case I, variation of frequency. For Case II, the decoloration per pulse is almost constant with varying the bust period from 0.25 to 1 ms, however, the range of energy per pulse is very small. For Case III, varying N-cycles, the decoloration per pulse decreased with energy per pulse for N-cycles from 1 to 30. In the region indicated by a red circle, i.e., at the same energy per pulse, the burst modes can give higher decoloration rates compared with uniform pulse.
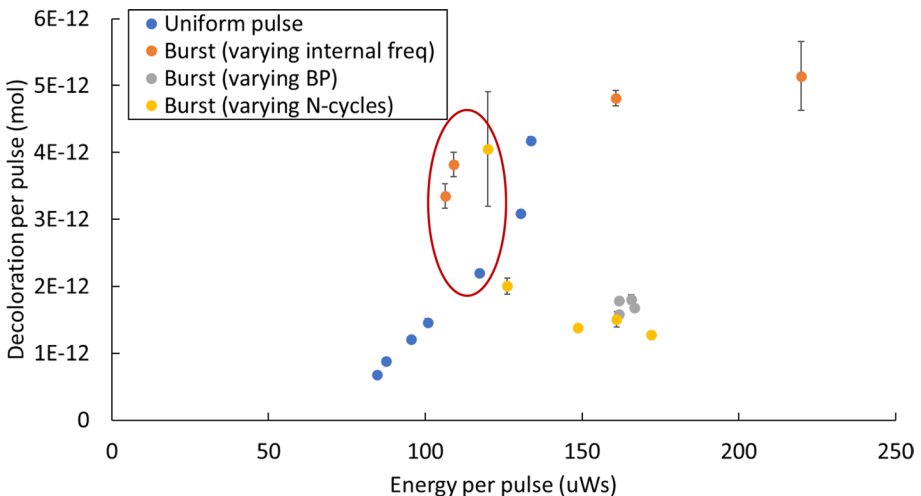

Fig. 12 Decoloration per pulse vs energy per pulse for 15 mL/min MB trials

Figure 13 shows the MB decoloration rate with variation of the total number of pulses. For uniform pulsing, the decoloration rate increased from 2.1×10^{-8} to 5.8×10^{-8} mol/s with an increase in total number of pulses from 5000 to 40,000 and then increased from 5.8×10^{-8} to 6.8×10^{-8} mol/s when the total number of pulses increased from 40,000 to 100,000. For Case I, when the internal frequency was varied in the range of 50–300 kHz, the decoloration rate decreased from 5.1×10^{-8} mol/s to 3.4×10^{-8} mol/s at the fixed 10,000 total number of pulses. For Case III, when the total number of pulses increased from 10,000 to 40,000, the decoloration rate increased from 1.7×10^{-8} mol/s to 6.4×10^{-8} mol/s. As shown in regions enclosed by red circles, several cases of the burst mode had higher decoloration rates than the uniform pulse with the same number of pulses.

Reaction Mechanism of H_2O_2 and MB Decoloration

Our previous work [24, 27], shows that the plasma propagates along the gas–liquid interface in our reactor. As shown in Fig. 14, water in contact with the plasma channel dissociates to form ·OH and ·H as shown in reaction R1. ·OH recombines to form H_2O_2 (R2) at the gas–liquid interfacial film and dissolves rapidly into the liquid phase. ·OH dissolved into the liquid phase reacts with MB to form a colorless complex (R3). As discussed in the previous sections, H_2O_2 was not affected by the pulse delivery method and linearly increased with total discharge power. MB decoloration was affected by the implementation burst mode and varying burst period resulted in higher decoloration than the uniform pulse. Table 3 shows Henry's law constant for H_2O_2 which is very high when compared with ·OH suggesting that H_2O_2 dissolves in liquid more easily than ·OH. In our previous work [33], it was demonstrated that H_2O_2 was the predominate carrier of ·OH and the production of H_2O_2 was not affected by introduction of MB in the liquid phase. This suggests that the burst mode is affecting the ·OH that go into the liquid phase but not the ·OH that produce H_2O_2. This implies that further work is required to determine the reason behind the effect of burst mode on ·OH dissolved in the liquid.
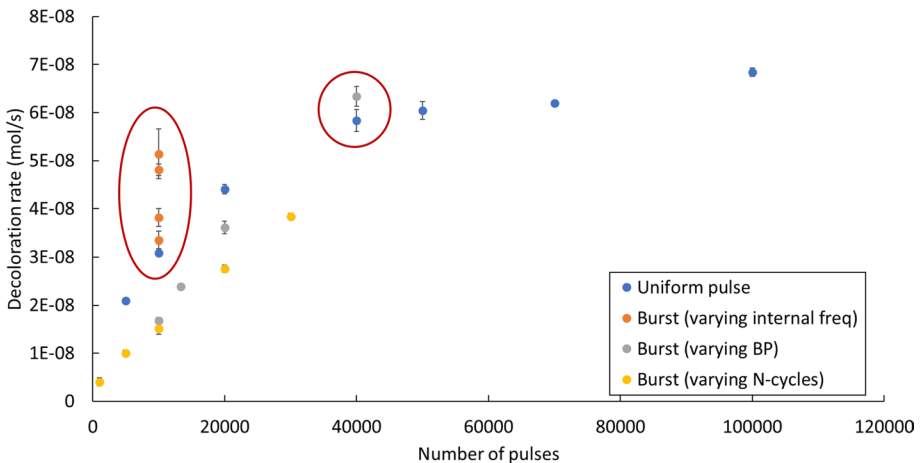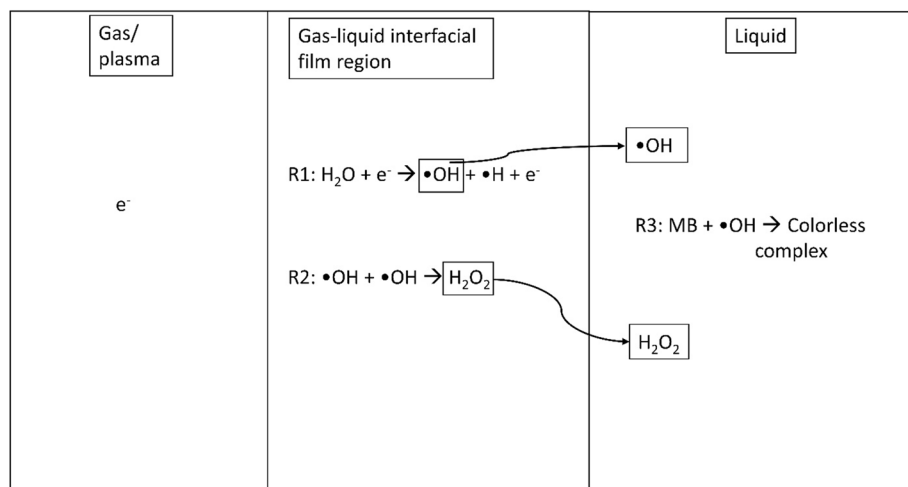

Fig. 13 Decoloration rate vs number of pulses for 15 mL/min MB trials

Table 3 Henry's law constants for H_2O_2 and •OH

Species	Henry's law constant (M atm^{-1})	Reference
H_2O_2	8.3×10^4	[34]
•OH	25	[35]

Fig. 14 Reaction mechanism pathway for the formation of H_2O_2 and MB decoloration

Conclusions

The application of nanosecond pulses in sequences of bursts were found to affect MB decoloration but not H_2O_2 generation in a flowing gas–liquid plasma reactor. Variation of the internal frequency, burst period, and N-cycles, did not affect the H_2O_2 generation when compared to uniform pulsing and in all cases the data showed a linear increase in generation with discharge power. This result suggests that in the range of parameters studied, the change in times between pulses is not sufficient to affect the chemical reactions that lead to generation of H_2O_2. In contrast, MB decoloration was affected by implementation of the different modes of applying the pulses in bursts. In terms of discharge power, in general the decoloration rate of MB was higher in the uniform pulsing case except for variation of the burst period, which had the same production rate at 6 W of discharge power. The linearly increasing trend of decoloration rate with discharge power for the variation of the burst period suggests that higher discharge power may lead to further enhancement over the uniform pulse delivery mode. Further work is needed to achieve these higher powers. When considering the energy in a pulse, the decoloration rate per pulse with variation of the internal frequency can be higher than that with the uniform pulsing, thus suggesting the burst mode can affect chemical reactions in the liquid. This work suggests that rurther work is needed to investigate a larger parameter space to explore the effects of bursts.

Availability of Data and Materials

There are no materials to provide. The data shown in the graphs can be provided in tabular form upon written request with explanation for the use of such data.

Declarations

Conflict of interest Professor Bruce R. Locke is an editor-in-chief of Plasma Chemistry and Plasma Processing.

Ethical Approval Not applicable.

References

1. Bruggeman PJ, Kushner MJ, Locke BR, Gardeniers JGE, Graham WG, Graves DB, Hofman-Caris RCHM, Maric D, Reid JP, Ceriani E, Rivas DF, Foster JE, Garrick SC, Gorbanev Y, Hamaguchi S, Iza F, Jablonowski H, Klimova E, Kolb J, Krcma F, Lukes P, Machala Z, Marinov I, Mariotti D, Thagard SM, Minakata D, Neyts EC, Pawlat J, Petrovic ZL, Pflieger R, Reuter S, Schram DC, Schroter S, Shiraiwa M, Tarabova B, Tsai PA, Verlet JRR, von Woedtke T, Wilson KR, Yasui K, Zvereva G (2016) Plasma-liquid interactions: a review and roadmap. Plasma Sources Sci Technol 25(5):053002
2. Brandenburg R, Bogaerts A, Bongers W, Fridman A, Fridman G, Locke BR, Miller V, Reuter S, Schiorlin M, Verreycken T, Ostrikov K (2019) White paper on the future of plasma science in environment, for gas conversion and agriculture. Plasma Processes Polym 16(1):e1700238
3. Weltmann K-D, Kolb JF, Holub M, Uhrlandt D, Simek M, Ostrikov K, Hamaguchi S, Cvelbar U, Cernak M, Locke B, Fridman A, Favia P, Becker K (2019) The future for plasma science and technology. Plasma Processes Polym 16(1):e1800118
4. Locke BR, Shih K-Y (2011) Review of the methods to form hydrogen peroxide in electrical discharge plasma with liquid water. Plasma Sources Sci Technol 20(3):034006
5. Patil BS, Wang Q, Hessel V, Lang J (2015) Plasma N-2-fixation: 1900–2014. Catal Today 256:49–66
6. Thanh PN, Sugai T, Tokuchi A, Jiang WH (2022) The effect of pulse discharge control on ozone production. IEEE Trans Plasma Sci 50(4):936–941
7. Kruger F, Lee H, Nam SK, Kushner MJ (2021) Electric field reversals resulting from voltage waveform tailoring in Ar/O-2 capacitively coupled plasmas sustained in asymmetric systems. Plasma Sources Sci Technol 30(8).
8. Zhu YF, Bo Y, Chen XC, Wu Y (2022) Tailoring electric field signals of nonequilibrium discharges by the deep learning method and physical corrections. Plasma Process Polymers 19(3).
9. Thanh PN, Sugai T, Tokuchi A, Jiang WH. The influence of pulse shape on the production of OH radicals by pulsed discharge. IEEE Trans Plasma Sci 5(1):199–204

10. Pourali N, Hessel V, Rebrov EV (2022) The effects of pulse shape on the selectivity and production rate in non-oxidative coupling of methane by a Micro-DBD reactor. Plasma Chem Plasma Process 42(3):619–640

11. Szulc M, Forster G, Marques-Lopez JL, Schein J (2022) Influence of pulse amplitude and frequency on plasma properties of a pulsed low-current high-voltage discharge operated at atmospheric pressure. Appl Sci-Basel 12(3).

12. Thana P, Kuensaen C, Poramapijitwat P, Sarapirom S, Yu LD, Boonyawan D (2020) A compact pulse-modulation air plasma jet for the inactivation of chronic wound bacteria: Bactericidal effects & host safety. Surface Coatings Technol, 400.

13. Shen SK, Yan JQ, Wang YA, Wang YS, Ding WD, Sun GX (2022) Stepwise development of atmospheric pressure plasma jet driven by bursts of high-voltage nanosecond pulses at multi-tens MHz. Plasma Sources Sci Technol 31(10).

14. Huang BD, Zhang C, Sun H, Sorokin DA, Tarasenko VF, Shao T (2022) Enhancement of hydrogen radical density in atmospheric pressure plasma jet by a burst of nanosecond pulses at 1 MHz. Plasma Sources Sci Technol 31(2).

15. Gromov M, Leonova K, Britun N, De Geyter N, Morent R, Snyders R, Nikiforov A (2022) Plasma nitrogen fixation in the presence of a liquid interface: role of OH radicals. Reaction Chem Eng 7(5):1047–1052

16. Wandell RJ, Locke BR (2014) Low-power pulsed plasma discharge in a water film reactor. IEEE Trans Plasma Sci 42(10):2634–2635

17. Wandell RJ, Wang H, Tachibana K, Makled B, Locke BR (2018) Nanosecond pulsed plasma discharge over a flowing water film: Characterization of hydrodynamics, electrical, and plasma properties and their effect on hydrogen peroxide generation. Plasma Processes Polymers 15(6).

18. Wang HH, Wandell RJ, Locke BR (2018) The influence of carrier gas on plasma properties and hydrogen peroxide production in a nanosecond pulsed plasma discharge generated in a water-film plasma reactor. J Phys D-Appl Phys 51(9):13

19. Wang H, Wandell RJ, Tachibana K, Vorac J, Locke BR (2019) The influence of liquid conductivity on electrical breakdown and hydrogen peroxide production in a nanosecond pulsed plasma discharge generated in a water-film plasma reactor. J Phys D-Appl Phys 52(7):075201.

20. Bresch S, Wandell R, Wang H, Alabugin I, Locke BR (2016) Oxidized derivatives of n-hexane from a water/argon continuous flow electrical discharge plasma reactor. Plasma Chem Plasma Process 36(2):553–584

21. Hsieh K, Wang HJ, Locke BR (2016) Analysis of a gas-liquid film plasma reactor for organic compound oxidation. J Hazard Mater 317:188–197

22. Xiong Y, Zhang Q, Wandell R, Bresch S, Wang H, Locke BR, Tang Y (2019) Synergistic 1,4-dioxane removal by non- thermal plasma followed by biodegradation. Chem Eng J 361:519–527.

23. Wandell RJ, Wang H, Bulusu RKM, Gallan RO, Locke BR (2019) Formation of nitrogen oxides by nanosecond pulsed plasma discharges in gas-liquid reactors. Plasma Chem Plasma Process 39(3):643–666

24. Bulusu RKM, Wandell RJ, Gallan RO, Locke BR (2019) Nitric oxide scavenging of hydroxyl radicals in a nanosecond pulsed plasma discharge gas liquid reactor. J Phys D-Appl Phys 52(50).

25. Hsieh KC, Wandell RJ, Bresch S, Locke BR (2017) Analysis of hydroxyl radical formation in a gas-liquid electrical discharge plasma reactor utilizing liquid and gaseous radical scavengers. Plasma Processes Polym 14(8):e1600171

26. Bulusu RK, Wandell RJ, Zhang Z, Farahani M, Tang Y, Locke BR (2020) Degradation of PFOA with a nanosecond-pulsed plasma gas-liquid flowing film reactor. Plasma Processes Polym 17(8):2000074

27. Bulusu RKM, Yatom S, Patterson CW, Wandell RJ, Locke BR (2022) Effects of frequency and pulse width on electron density, hydrogen peroxide generation, and perfluorooctanoic acid mineralization in a nanosecond pulsed discharge gas-liquid plasma reactor. J Vac Sci Technol A Vac Surf Films 40(6):063001

28. Wandell RJ, Bresch S, Wang H, Babicky V, Lukes P, Locke BR (2020) The effects of pulse frequency on chemical species formation in a nanosecond pulsed plasma gas-liquid film reactor. Int J Plasma Environ Sci Technol 14(e01008):1–9.

29. Vinson E, Bulusu R, Wandell R, Locke B (2022) Chemical reduction by aqueous electrons in a nanosecond pulsed discharge gas-liquid plasma reactor. Int J Plasma Environ Sci Technol 16(2):e02005 (15 pp).

30. Reddy PMK, Raju BR, Karuppiah J, Reddy EL, Subrahmanyam C (2013) Degradation and mineralization of methylene blue by dielectric barrier discharge non-thermal plasma reactor. Chem Eng J 217:41–47

31. Eisenberg GM (1943) Colorimetric determination of hydrogen peroxide. Ind Eng Chem Anal Ed 15(5):327–328
32. Tao S, Guangsheng S, Ping Y, Jue W, Weiqun Y, Yaohong S, Shichang Z (2006) An experimental investigation of repetitive nanosecond-pulse breakdown in air. J Phys D Appl Phys 39(10):2192
33. Hsieh KC, Wandell RJ, Bresch S, Locke BR (2017) Analysis of hydroxyl radical formation in a gas-liquid electrical discharge plasma reactor utilizing liquid and gaseous radical scavengers. Plasma Processes Polym 14(8):14
34. O'Sullivan DW, Lee M, Noone BC, Heikes BG (1996) Henry's law constant determinations for hydrogen peroxide, methyl hydroperoxide, hydroxymethyl hydroperoxide, ethyl hydroperoxide, and peroxyacetic acid. J Phys Chem 100(8):3241–3247
35. Arangio AM, Slade JH, Berkemeier T, Pöschl U, Knopf DA, Shiraiwa M (2015) Multiphase chemical kinetics of OH radical uptake by molecular organic markers of biomass burning aerosols: humidity and temperature dependence, surface reaction, and bulk diffusion. J Phys Chem A 119(19):4533–4544